DEVICE PHYSICS OF CRYSTALLINE SOLAR CELLS*

MARK S. LUNDSTROM
School of Electrical Engineering, Purdue University, West Lafayette, IN 47907 (U.S.A.)

(Received November 16, 1987; accepted December 22, 1987)

Summary

High material quality is a prerequisite for achieving high conversion efficiencies, but cells must be carefully designed to maximize performance. Very high conversion efficiencies are now being achieved in two quite different semiconductors, silicon and GaAs. The internal device physics of crystalline silicon and GaAs cells are compared and contrasted in this paper. The paper illustrates how detailed device simulation is used to examine the internal performance of cells, identify loss mechanisms and assess design options.

1. Introduction

Record high conversion efficiencies are now being reported for both crystalline silicon and gallium arsenide solar cells. High material quality was a prerequisite for achieving these high efficiencies, but cell design was also a crucial factor. The design of a solar cell is based on the properties of the semiconductor, the constraints imposed by the technology, and on an understanding of the cell's internal device physics. The purpose of this paper is to discuss, compare and contrast the device physics of silicon and gallium arsenide cells. The paper does not attempt a comprehensive review of silicon and GaAs cells; its emphasis is on the device physics that confronts the cell designer. A review of how such high efficiencies were achieved in two quite different semiconductors demonstrates that there is no single, best solar cell design but, rather, that solar cell designs evolve as dominant recombination losses are identified. The paper will also illustrate how physical device simulation is used to identify loss mechanisms and to guide device design.

2. Cell design fundamentals

We begin with a brief review of the basic concepts underlying the design of high-efficiency cells. The simple expression

*Paper presented at the 8th Photovoltaic Advanced Research and Development Project Review Meeting, Denver, CO, U.S.A., November 15 - 18, 1987.

0379-6787/88/$3.50

$$\eta = \frac{J_{SC} V_{OC} FF}{P_{inc}/A} \tag{1}$$

shows that high efficiency results by maximizing short-circuit current J_{SC} and open-circuit voltage V_{OC} while maintaining a high fill factor (FF). The selection of a semiconductor is a compromise; to maximize short-circuit current, a small band gap should be selected, but for high open-circuit voltage, a large band gap is needed. The band gaps of silicon and GaAs are nearly optimum for the solar spectrum; both cells show limit conversion efficiencies above 30% at one sun and above 35% at 500 suns [1].

The object of cell design is to approach the cell's thermodynamic limit by maximizing the number of optically-generated carriers while minimizing recombination losses. To achieve high efficiencies, 98% of the available photons should be absorbed. For GaAs, a layer of semiconductor about 4 μm thick is adequate, but for silicon, a layer 1500 μm thick is required. For such thick silicon cells, the electrical performance would be degraded by recombination losses. Much of the recent improvement in silicon performance is due to the use of light-trapping techniques which makes the cell appear optically thick yet electrically thin. There has also been much progress in sophisticated antireflection coatings, texturizing and grid design which have resulted in reflection plus shadowing losses below 3%. Successful cell design consists of identifying, quantifying, then suppressing the important recombination mechanisms. The designer needs the ability to examine the cell's internal recombination rate. Unfortunately, electrical measurements tend to reflect the integrated recombination rate and cannot therefore identify the importance of specific internal mechanisms. Experiments to isolate and quantify various mechanisms can be performed, but they are difficult and time-consuming. An alternative approach which involves the use of a detailed, physical device model is discussed next.

3. Physical device simulation

The performance of a cell is described by Poisson's equation and by the electron and hole continuity equations which comprise three coupled non-linear equations in three unknowns (electrostatic potential, electron concentration and hole concentration). Under well-known simplifying assumptions (*e.g.* simple doping profiles, complete ionization of dopants, low-level injection etc.) the governing equations can be simplified and closed-form solutions obtained, but cells often operate under conditions that invalidate many simplifying assumptions. Moreover, the continued quest for higher efficiencies demands more accurate and detailed modeling of the device.

Physical device simulation consists of solving the governing equations directly by using a digital computer [2, 3]. The only approximations involved are numerical (*e.g.* derivatives are approximated by finite differences). The

accuracy of the model is limited not by the ability to solve the governing equations, but by knowledge of the physics and the values of various materials parameters. Since the solution is obtained at each point within the device, not simply at its terminals, the internal operation of the device can be probed at will. For crystalline silicon cells, computer codes that solve the governing equations in one and two dimensions are now widely available. Confidence in the predictive ability of these codes was established by comparing simulations with experiments. The successes and failures of these comparisons deepened the understanding of silicon cell device physics and focused experimental work on topics of most concern to device design. After a decade of such work, confidence in the codes is high; they now serve as reliable guides for cell design. For GaAs and "newer" materials, confidence in the physical models is not yet as high, but trends can be modeled and the merits of various designs gauged. These models are improving as knowledge of device physics and parameter values improves.

4. Device physics of silicon cells

In this section, we make use of computer simulation to examine and compare the internal device physics of two different concentrator cells. The first cell considered is similar to the Sandia, p on n cell developed in the early 1980s [4]. Next, we examine the internal device physics of a backside-contact cell similar to the Stanford design [5]. Identical, high-quality material is assumed for both of the cells to assess the role of device design on cell performance.

The Sandia-like p on n cell is displayed in Fig. 1; it is fabricated in a 0.3 Ω cm substrate 305 μm thick. The p^+ emitter is 0.4 μm thick with a peak concentration of 1.5×10^{20} cm^{-3}, and the back-surface field is a diffused junction 1.0 μm thick with a peak doping of 5.0×10^{19} cm^{-3} (complementary error functions were used for both profiles). The Shockley–Read–Hall (SRH) lifetimes were modeled by

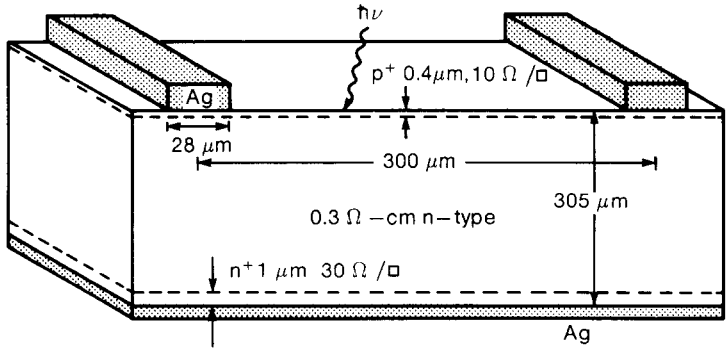

Fig. 1. Physical structure of the Sandia-like [4] p on n concentrator cell.

$$\tau = \frac{\tau_o}{1 + N/N_c} \tag{2}$$

where τ_o, the SRH lifetime in intrinsic material, was taken to be 1000 μs and N_c, which controls how the SRH lifetime degrades with doping, was set to 7.1×10^{15} cm^{-3}. Auger recombination was also modeled and the passivated surfaces were characterized by a surface recombination velocity of 10 cm s^{-1}.

The results of a two-dimensional physical simulation of the p on n cell are summarized in Table 1; the simulated conversion efficiency under concentration exceeds 20%. Simulation results show that 80% of the available photons are collected. About half of the lost photocurrent is caused by reflection and shadowing; the other half of the loss is about equally divided between carrier recombination within the cell (about 4%) and transmission of above-band-gap photons through the 300 μm thick cell.

Figure 2 summarizes the recombination losses at V_{OC} for this cell as revealed by physical simulation. The relatively small (about 4%) contribution of base recombination to the dark current should be noted. The heavy base doping, in contrast with earlier cell designs, effectively suppresses forward-biased injection of holes into the base. The dominant V_{OC}-loss mechanism is recombination within the thin, heavily doped p-type emitter. Since the emitter is well passivated, this current component is due to injected minority carriers recombining within the volume of the emitter and can be described by

$$J_E(p^+ \text{ bulk}) = q\frac{n_{iE}^2}{N_A}\frac{W_E}{\tau} \tag{3}$$

where n_{iE} is the intrinsic carrier concentration in the emitter, N_A is the average doping, W_E is the width of the emitter and τ is the minority carrier lifetime. The emitter component of the dark current dominates for two reasons. Firstly, so-called band-gap narrowing effects effectively shrink the band gap within the heavily doped emitter, so that n_{iE} may greatly exceed its value in intrinsic silicon n_{io} [6]. In the heavily doped emitter, n_{iE}^2 may

TABLE 1

Simulated performance of the p on n silicon concentrator cell at T = 24 °C under 180× air mass (AM) 1.5 direct suns

Cell parameter	*Value*
V_{OC} (V)	0.757
J_{SC} (A cm^{-2})	5.52
FF (%)	79
η (%)	22
J_{SC}/J_L (max) (%)	80
Internal conversion efficiency (%)	96
Shadow plus reflection (%)	9.4

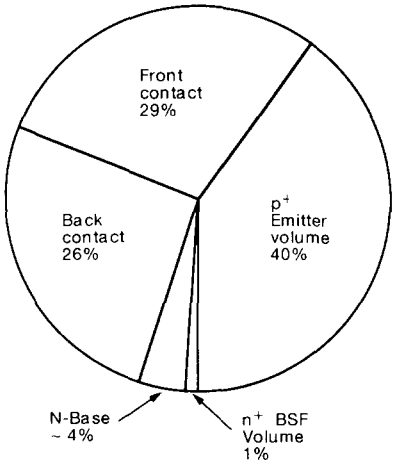

Fig. 2. Recombination analysis of Sandia-like p on n silicon concentrator cell at V_{OC}.

be several times the value in lightly doped silicon. Secondly, the emitter recombination rate is high because of the dominance of Auger recombination in the heavily doped emitter. The Auger-limited, low injection minority carrier lifetime

$$\tau = \frac{1}{C_p N_A^2} \tag{4}$$

is only 1 ns in p-type silicon doped to 1×10^{20} cm^{-3}.

Figure 2 also shows that more than half of the recombination losses in this cell arise from minority carriers recombining at the metal contacts. These losses are a consequence of band-gap narrowing which causes a substantial injection of minority carriers into the heavily doped regions where they can recombine at the metal contacts. The back-surface field does improve the performance of this cell, but it is not a perfect minority carrier mirror; a number of minority carriers reach the back metal contact and recombine there.

According to these simulation studies, silicon cell design should be directed at suppressing recombination in the emitter volume and at the metal contacts. Further increases in J_{SC} are possible if the already low shadowing losses can be eliminated and if the high internal quantum efficiency can be improved. The Stanford backside point contact cell [5] achieves both objectives. In the Stanford cell, both the p- and n-type diffused junctions are reduced to small dots on the backside of the wafer, so grid shadowing losses are eliminated, and Auger recombination in the volume of the diffused regions is reduced, as is recombination at the metal–semiconductor contacts. The light base doping is used to maximize Shockley–Read–Hall lifetimes; its resistance is low because the base operates in high level injection. To maintain a high internal collection efficiency and open-circuit voltage, the cell must be thin. Light-trapping techniques are then essential to make the semiconductor appear optically thick.

TABLE 2

Simulated performance of the Stanford backside point contact cell (T = 24 °C, AM 1.5 direct normal, at 180×)

Cell parameter	*Value*
V_{OC} (V)	0.826
J_{SC} (A cm^{-2})	6.39
FF (%)	85
η (%)	30.1
J_{SC}/J_L (max) (%)	93
Internal conversion efficiency (%)	99.5
Shadow plus reflection loss (%)	0

Table 2 summarizes the electrical performance of the backside point contact cell under concentration. The very substantial reduction of recombination losses achieved by reducing the volume of the heavily doped regions and the area of the metal-semiconductor contacts is reflected in the especially high open-circuit voltage. The recombination analysis at V_{OC} for this cell, displayed in Fig. 3, shows that the p^+ volume, the n^+ volume and the metal contacts contribute about equally to the recombination losses. Recombination losses associated with the intrinsic cell are so low that parasitic losses associated with recombination at the perimeter of the cell should be considered. Because perimeter recombination was not simulated and the extrinsic series resistance was assumed to be zero, the simulated efficiency is about two percentage points above the observed value.

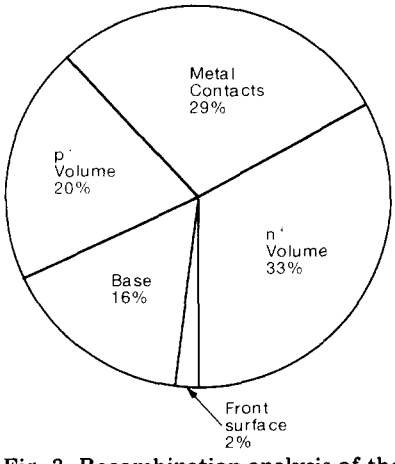

Fig. 3. Recombination analysis of the Stanford-like point contact cell at V_{OC}.

5. Device physics of GaAs cells

Although very high efficiencies have been reported for gallium arsenide solar cells under both one sun and concentration [7, 8], our understanding

of their internal device physics is not mature by silicon standards. The most common cell design, the p on n heteroface displayed in Fig. 4, has not changed appreciably for several years, but efficiencies have continued to rise as antireflection coatings, material quality and fabrication techniques have improved [7]. Experiments to probe the internal device physics have recently begun (*e.g.* refs. 9 and 10), as has the serious use of physical device simulation. Simulation now describes cell performance reasonably well and can be used to assess the potential of design alternatives.

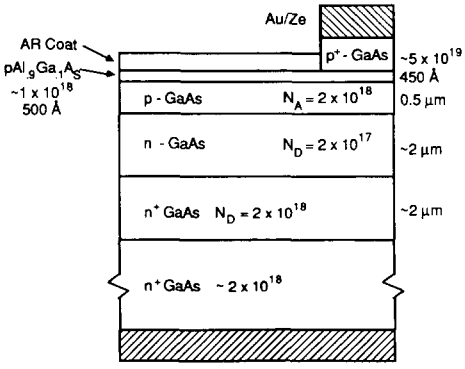

Fig. 4. Physical structure of the Spire-like p on n GaAs heteroface cell [9].

The basic cell structure, displayed in Fig. 4, consists of a p^+ emitter and an n-type base. The heavily doped buffer layer serves as a minority carrier mirror, and the wide band gap $Al_{0.9}Ga_{0.1}As$ window layer passivates the front surface. Numerical simulations by PUPHS [2] demonstrate that the band gap of the window (about 2 eV) permits a substantial photogeneration of carriers (about 5% of the available photons are absorbed in a window 500 Å thick). A few per cent of the available photons are also generated in the n^+ buffer layer. The simulated internal quantum efficiency is compared with a typical measured value [10] in Fig. 5. The drop in quantum efficiency at short wavelength is due to absorption in the window layer, but the window layer is not dead. A front surface recombination velocity at the AlGaAs surface of 5×10^6 cm s^{-1} (which is somewhat below the value of about 10^7 cm s^{-1} typical of a bare GaAs surface) is needed to model the short wavelength quantum efficiency. About one-half of the carriers photogenerated in the window layer are collected. The long wavelength quantum efficiency is quite high; very long base lifetimes are implied (a value of 15 ns was used in the simulation). The peak quantum efficiency, typically 90% - 95%, is very high, but contrasts with the results for silicon in which the quantum efficiency routinely peaks very near 100%. The peak quantum efficiency can be explained by assuming a recombination velocity at the heteroface of several times 10^4 cm s^{-1} to a few times 10^5 cm s^{-1}, which is substantially above the 10^4 cm s^{-1} commonly assumed as an upper limit. But other explanations, such as a parasitic absorption mechanism that does not generate carriers, cannot be ruled out.

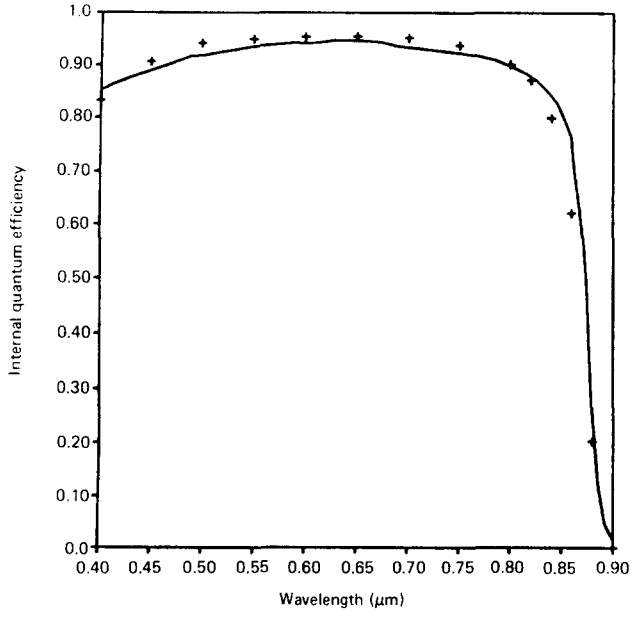

Fig. 5. Internal quantum efficiency *vs.* wavelength for a typical p on n heteroface cell (——, PUPHS simulation; + + +, from ref. 11).

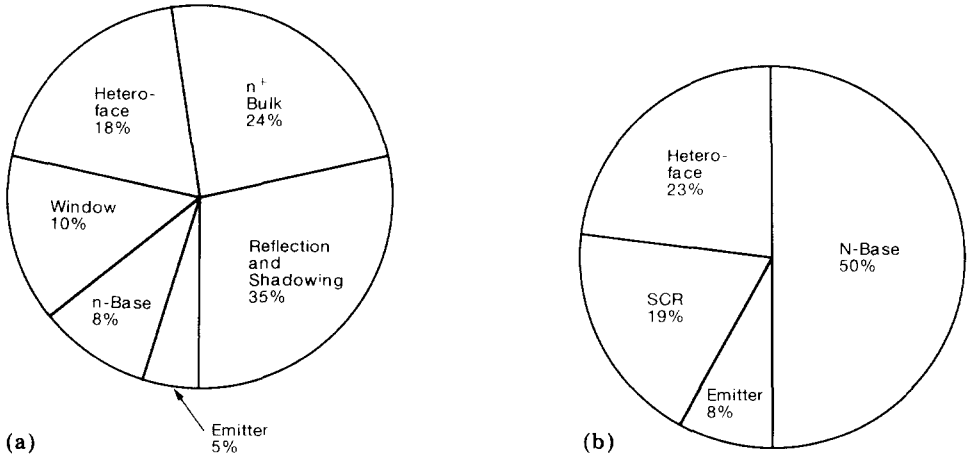

Fig. 6. (a) Short-circuit current loss analysis of the p on n GaAs heteroface cell. In the simulated cell, 13% of the available photogenerated carriers are lost. This chart shows where those photons are lost; (b) recombination analysis of the p on n GaAs heteroface cell at the one-sun V_{OC}.

Short-circuit current losses for this cell are summarized in Fig. 6(a). Reflection and shadowing by the top metal grid are the largest component of optical loss. The sizable loss contributed by the n^+ buffer layer and substrate indicates that the cell's active layer is not thick enough optically, but

increasing its thickness would degrade the open-circuit voltage (in this regard, GaAs cells could benefit from light-trapping techniques like those employed for silicon cells). The loss contributed by the heteroface reflects the high interface recombination velocities implied by the peak internal quantum efficiency.

Recombination losses at open-circuit voltage are summarized in Fig. 6(b). In contrast to the silicon p on n cells, the GaAs cell's dark current is base-dominated. The emitter doping for the GaAs cell is not extremely high, so minority carrier electrons are injected into the emitter. But injection of minority carriers into the emitter does not have the dire consequences that it does for silicon cells because the metal contacts are passivated by the heteroface and the lifetimes in the emitter are relatively long (about 2 ns). The performance of the n^+ back-surface field is not severely compromised because majority carrier degeneracy is strong in n-type GaAs and acts to counter band-gap shrinkage. For n–p cells, however, the performance of p^+ back-surface fields should be degraded by band gap shrinkage, which may explain why heterojunction back-surface fields have proved effective for such cells [12]. The simulations show a sizable, though not dominant, emitter component to the dark current which is a consequence of the relatively high heteroface recombination velocity used to match the low peak internal quantum efficiency. Strong variations of dark current with emitter design should not be observed until the dominant loss, base recombination, is suppressed.

Table 3 summarizes the simulated performance of the Spire-type p on n heteroface cell at one sun and the performance of a similar cell (with a redesigned grid) under concentration. These results were obtained with a two-dimensional, AlGaAs–GaAs simulator. The table shows that about 87% of the available photons are collected; in the very best silicon cells the corresponding fraction exceeds 95%. The cell's dark current is primarily caused by recombination in the n-type base. Under concentration, simulations of a similar cell (with a very conservative metal grid that results in 11% shadowing) show a conversion efficiency of more than 27%.

When we consider optimizing this cell, it is clear that the first objective must be to raise the fraction of available carriers that are collected. The reason for the low peak internal quantum efficiency (low, that is, by silicon standards) must first be identified. As discussed previously, a tentative explanation is that the heteroface recombination velocity exceeds 10^4 cm s^{-1}. When this value is lowered to 10^4 cm s^{-1}, simulations show nearly 100% peak internal quantum efficiency. Modest improvements in cell performance can also be achieved by reducing the dark current. To reduce dark currents, the focus should be on suppressing the base current, which is most easily accomplished by increasing the base doping (if the diffusion length in the base can be maintained). No fundamental mechanism limits the hole lifetime in n-GaAs until the doping exceeds 10^{18} cm^{-3} [14 - 16], so base dopings higher than 2×10^{17} cm^{-3} could be employed. This approach has been adopted in the Varian p on n heteroface cell [8]. The use of heterojunction back-surface fields to suppress dark current might also be considered, but in

TABLE 3

Simulated performance of the p on n heteroface GaAs cell

Cell parameter	*1 sun*[a]	*500 suns*[b]	*500 suns*[c]
V_{OC} (V)	1.038	1.19	1.22
J_{SC} (mA cm^{-2})	27.4	10.9	11.4
FF (%)	86	87	86
η (%)	24.6	27.1	39.0
J_{SC}/J_L (max) (%)	87	81	85
Internal CE (%)	90	89	88
Shadow plus reflection (%)	5	11	6

All simulations were performed at 25 °C.
[a]Refers to the cell displayed in Fig. 4 under an AM 1.5 global spectrum normalized to 100 mW cm^{-2} [13].
[b]Refers to a similar cell at 500 AM 1.0 direct normal suns.
[c]Refers to an optimized cell as described in the text.

this case the base must be thickened to prevent a loss of photocurrent [11]. Since the back-surface field will be located more than a diffusion length beyond the junction, significant benefits are not expected for heterojunction back-surface fields in p on n cells. Finally, we note that 1 ns lifetimes can be maintained in the p-type emitter for doping densities near 10^{19} cm^{-3} [14, 17, 18]. For such lifetimes, the short wavelength internal quantum efficiency does not suffer (recent experiments provide confirmation [10]). The implication is that the emitter doping can be substantially raised to lower the emitter sheet resistance without sacrificing internal quantum efficiency.

Table 3 also shows the simulated performance of an optimized cell, which was designed as discussed above. The cell is identical to that displayed in Fig. 4 except that the peak internal quantum efficiency has been raised to nearly 100% by lowering the heteroface recombination velocity to 1×10^4 cm s^{-1}, the emitter doping has been raised to 8×10^{18} cm^{-3} and the base doping has been raised to 5×10^{17} cm^{-3}. The lowered sheet resistance of the p^+ emitter allowed the front grid to be redesigned to lower shadowing losses to 6% without degrading the fill factor. A significant gain in performance is predicted; the cell shows a conversion efficiency of 29%. Even with this very high conversion efficiency, the short-circuit current represents only 85% of the available photons. Conversion efficiencies in excess of 30% are achievable if the short-circuit current performance of GaAs cells can be raised.

6. Conclusions

In this paper the internal device physics of a number of different solar cell designs in two different crystalline semiconductors has been studied. A unifying theme of the discussion was the role that detailed device simulation plays in guiding solar cell design. Some general conclusions regarding the

design of silicon, GaAs and all crystalline cells can be derived from this discussion. The first is the importance of maximizing short-circuit current; the very best silicon cells make use of long-lifetime material and light-trapping techniques to collect about 96% of the available photocurrent [5]. This appears to be the key area of opportunity for improving the already high efficiency of GaAs cells (the best GaAs cells collect about 88% of the available photocurrent [7]). Band-gap narrowing effects play a dominant role in silicon cell design; they enhance the injected minority carrier concentration so that Auger recombination and recombination at the metal contacts dominates. Much of silicon cell design focuses on designing around heavy doping effects. For GaAs cells, band-gap narrowing may occur (especially in p^+ GaAs), but its consequences are not so dire. Both materials display high fill factors (typically just under 80% for silicon at one sun and somewhat over 80% for GaAs). A conversion efficiency of 30% under concentration appears to be an achievable goal for both silicon and GaAs cells.

Acknowledgments

The author is indebted to E.K. Banghart for performing the simulations of silicon cells and to P.D. DeMoulin for the GaAs simulations. He also benefited from extensive discussions with S.P. Tobin of Spire Corporation and J.M. Gee of Sandia National Laboratories. Development of the simulation tools described in this paper was supported by Sandia National Laboratories; experimental studies to verify the GaAs models were supported by the Solar Energy Research Institute.

References

1 C. H. Henry, Limiting efficiencies of ideal single and multiple energy gap terrestrial solar cells, *J. Appl. Phys., 51* (1980) 4494 - 4500.
2 M. S. Lundstrom and R. J. Schuelke, Numerical analysis of heterostructure devices, *IEEE Trans. Electron Devices, 30* (1983) 1151 - 1159.
3 J. L. Gray and R. J. Schwartz, Two-dimensional computer simulation of single crystal silicon concentrator cells, *Proc. 17th IEEE Photovoltaic Specialists' Conf., Kissimmee, FL, 1984*, IEEE, New York, 1984, pp. 1297 - 1302.
4 R. D. Nasby, C. M. Garner, F. W. Sexton, J. L. Rodriguez, B. H. Rose and H. T. Weaver, High efficiency p^+–n–n^+ silicon concentrator solar cells, *Sol. Cells, 6* (1982) 49 - 58.
5 R. A. Sinton, Y. Kwark, J. Y. Gan and R. M. Swanson, 27.5-Percent efficient silicon concentrator solar cells, *IEEE Electron Dev. Lett., 7* (1986) 567 - 569.
6 J. W. Slotboom and H. C. de Graaff, Measurements of bandgap narrowing in Si bipolar transistors, *Solid-State Electron., 19* (1976) 857 - 862.
7 S. P. Tobin, C. Bajgar, S. M. Vernon, L. M. Goeffroy, C. J. Keavney, M. M. Sanfacon, V. E. Haven, M. B. Spitzer and K. A. Emery, A 23.7 percent efficient one-sun GaAs solar cell, *Proc. 19th IEEE Photovoltaic Specialists' Conf., New Orleans, LA, May 4 - 8, 1987*, IEEE, New York, 1987, pp. 1492, 1493.

8 H. C. Hamaker, C. W. Ford, J. G. Werthen, G. F. Virshup, N. R. Kaminar, D. L. King and J. M. Gee, 25% Efficient magnesium-doped AlGaAs/GaAs solar concentrator cells, *Appl. Phys. Lett., 47* (1985) 762 - 764.
9 M. S. Lundstrom, M. R. Melloch, R. F. Pierret, P. D. DeMoulin, D. P. Rancour, C. S. Kyono and M. S. Carpenter, Basic studies of III–V high-efficiency cell components, *Technical Report TR-EE 87-33*, School of Electrical Engineering, Purdue University, West Lafayette, IN, September, 1987.
10 S. P. Tobin, Spire Corporation, private communication.
11 P. D. DeMoulin, M. S. Lundstrom and R. J. Schwartz, GaAs concentrator cells: design options and constraints, *Proc. 18th IEEE Photovoltaic Specialists' Conf., Las Vegas, NV, 1985*, IEEE, New York, 1985, pp. 321 - 326.
12 R. P. Gale, John C. C. Fan, G. W. Turner and R. L. Chapman, *Proc. 17th IEEE Photovoltaic Specialists' Conf., Kissimmee, FL, 1984*, IEEE, New York, 1984, p. 1422.
13 R. Hulstrom, R. Bird and C. Riordan, Spectral solar irradiance data sets for selected terrestrial conditions, *Sol. Cells, 15* (1985) 365 - 391.
14 C. J. Hwang, *J. Appl. Phys., 42* (1971) 4408 - 4413.
15 C. J. Hwang, *Phys. Rev. B, 6* (1972) 1355 - 1359.
16 A. Huag, *J. Phys. C, 16* (1983) 4159 - 4172.
17 H. C. Casey, Jr., and M. B. Panish, *Heterostructure Lasers*, Academic Press, New York, 1978.
18 R. J. Nelson and R. G. Sobers, *J. Appl. Phys., 49* (1978) 6103 - 6108.